Turkish Journal of Electrical Engineering & Computer Sciences

http://journals.tubitak.gov.tr/elektrik/

Research Article

Turk J Elec Eng & Comp Sci
(2016) 24: 2994 – 3010

doi:10.3906/elk-1403-269

# Sensorless field oriented control of nonsinusoidal flux-distribution permanent magnet synchronous motor with a FEM based ANN observer

**Eyyüp ÖKSÜZTEPE[1,*], Zeki OMAÇ[2], Mehmet POLAT[3], Hakan ÇELİK[3], Ahmet Hakan SELÇUK[4], Hasan KÜRÜM[5]**

[1]Department of Computer Engineering, Faculty of Engineering, Tunceli University, Tunceli, Turkey
[2]Department of Electrical–Electronics Engineering, Faculty of Engineering, Tunceli University, Tunceli, Turkey
[3]Department of Mechatronics Engineering, Faculty of Engineering, Fırat University, Elazığ, Turkey
[4]Department of Electrical–Electronics Engineering, Faculty of Engineering and Architecture, Balıkesir University, Balıkesir, Turkey
[5]Department of Electrical–Electronics Engineering, Faculty of Engineering, Fırat University, Elazığ, Turkey

**Received:** 26.03.2014 • **Accepted/Published Online:** 23.01.2015 • **Final Version:** 15.04.2016

**Abstract:** The sensorless vector control of a nonsinusoidal flux-distribution permanent magnet synchronous motor (PMSM) has been performed by a trained artificial neural network (ANN) using flux data obtained from the finite element method (FEM). A more sensitive rotor position has been estimated by using the fluxes of each of the three phases of the PMSM. In the proposed approach, magnet flux of the nonsinusoidal PMSM has been calculated by FEM for every single degree. Rotor position and speed values have been estimated by training an ANN with this information. The experimental results obtained by DS1103 development kit have proved the validity of the proposed approach.

**Key words:** PMSM, sensorless Control, DSP, AC drivers

## 1. Introduction

In recent years, permanent magnet synchronous motors (PMSMs) have attracted increasing interest because of their low inertia, high power rate, and high efficiency. Rotor position information is needed by the drivers of this type of motor to synchronize the fields of rotor and stator. This information is obtained from electromechanical or optical sensors. However, these sensors not only reduce the reliability, but also increase cost and dimensions. That is why sensorless control methods are preferred, with which the estimations of rotor position and speed are made from motor current and voltage information instead of sensors [1–3].

There are two types of air gap flux of permanent magnet AC motors according to their wave shapes: sinusoidal and trapezoidal. In the literature, the motors having sinusoidal flux-distribution are PMSMs and those having trapezoidal flux-distribution are brushless DC motors. Only two of the three phase windings are excited at the same time and the fields of rotor and stator are synchronized at every 60° electrical angle in the sensorless control of brushless DC motors. A continuous and accurate synchronization is needed between the rotor and stator fields in the sensorless control of PMSMs [4]. Therefore, the sensorless control of PMSMs is more complicated than that of brushless DC motors.

The sensorless control of a PMSM varies with the rotor type. Interior motors have saliency and this can be used to calculate the rotor position. The signal injection method also depends on this saliency [5]. The signal

*Correspondence: eoksuztepe@tunceli.edu.tr

injection method is successful at low speeds; however, it cannot be used at high speeds since higher frequency signals are necessary. Moreover, this method generates torque ripples and noise. Furthermore, this method cannot be used for surface magnet synchronous motors under normal conditions since there is no saliency [6]. The speed and position information of the PMSM can be obtained from the back emf induced by the rotor magnets on the stator windings. This method is named as the back emf method [7–9]. However, this method is unsuccessful at low speeds since the induced emf is so small that it cannot be separated from noise, while it is successful at middle and high speeds. The flux linkages of the stator windings are proportional to the back emf and they are a function of the rotor position. Many methods have been proposed in the literature to estimate the flux linkages. The magnet flux is estimated by using the reactive power feedback in [10]. Flux of the magnet has been estimated by using an extended Kalman filter in [11]. Magnet flux is estimated by using stator current estimation error and an ANN in [12]. Magnet flux is predicted by using stator inductances, magnet flux steady state voltage equations, and flux harmonics in [13]. In [14], stator flux is estimated by using a reduced-order rotor flux observer. However, all these methods are complicated and computationally expensive.

In PMSMs, the air gap flux is not an exact sinusoidal or trapezoidal because of the influences of slots and saturation [15]. The stator windings must be distributed such that moving rotor magnets induce a sinusoidal voltage on them. In practice, the stator windings can be distributed as the number of slots allow. In addition, the saturation occurring in some regions of the motor plates prohibits the flux to be an exact sinusoidal. Furthermore, the skew rate at the stator slots influences the waveform of the flux linkage.

In the speed and position sensorless control model of PMSMs, it is assumed that the motor air gap flux variation is an exact sinusoidal. The use of this assumption in the position and speed sensorless control of PMSMs causes ripples in torque and reduces performance. The rotor position of the PMSM having nonsinusoidal flux-distribution can be predicted after determination of the flux harmonic coefficients by measurements [15,16], but the harmonic degree must be limited since the amount of calculations for the digital signal processor becomes large. The flux waveform can be determined by measuring back emfs induced in the stator windings of the motor while not exciting the windings and with rotation by another motor. In order to get back emfs great enough to separate from noise, the motor must be rotated at high speeds. In this case it is necessary to get enough data to determine the flux waveform correctly. Measurement errors and noise bring difficulties in obtaining flux waveform correctly.

The flux waveform, which depends on the motor geometry, can be calculated accurately by using FEM. In fact, it is not new to use FEM in motor control. In [17], it is recommended to improve servo motor control with FEM. Furthermore, there are many studies on reducing torque ripples in the control of PMSMs by using the data obtained from FEM [18–20].

In this work, the 2D FEM analysis of the PMSM has been performed and flux waveform has been determined by considering the skew in the stator slots. The flux waveform, which is a function of the rotor position, has been modelled with a positive-feedback 3-layer ANN and all the flux harmonics have been considered in the calculations. The rotor position of the PMSM having an arbitrary flux waveform can be estimated by this method. The problems of integrator shift and variations in motor parameters during the estimation process are overcome with the help of a controller. The real-time application of the proposed method has been conducted with the help of a DS1103.

## 2. The simplified mathematical model of the PMSM

The voltage relations for the PMSM are given in Eqs. (1) and (2) in the rotating reference plane.

$$v_q = r_s i_q + p\lambda_q + \omega_r \lambda_d \tag{1}$$

$$v_d = r_s i_d + p\lambda_d - \omega_r \lambda_q \tag{2}$$

Here $v_q$, $i_q, \lambda_q V_q$ and $v_d$, $i_d, \lambda_d$ are the q and d axis voltages, currents, and flux linkages, respectively; $p$is the derivative operator; and $\omega_r$ is the electrical angular speed of the rotor.

The d and q axis flux linkages are defined by Eqs. (3) and (4).

$$\lambda_q = L_q i_q \tag{3}$$

$$\lambda_d = L_d i_d + \lambda_m \tag{4}$$

Here $\lambda_m$ is the flux generated by permanent magnets.

The electrical torque equation of the PMSM is Eq. (5).

$$T_e = \frac{3P}{2}\left[\lambda_m i_q + (L_d - L_q)\, i_q i_d\right] \tag{5}$$

$P$ represents the number of pole pairs. For cylindrical - rotor surface - magnet motors. $L_d = L_q = L_\alpha = L_\beta = L$. The mechanical equation of the motor is

$$T_e = Jp\omega_{rm} + B\omega_{rm} + T_y \tag{6}$$

Here $\omega_{rm}$, $J$, and $T_L$ represent angular speed, inertia of the rotor, and load torque, respectively. The electrical and mechanic properties of the motor to be investigated are given in the Appendix.

All these equations assume that the flux waveform is exactly sinusoidal, but the flux has actually some harmonics.

## 3. Modeling the PMSM with FEM

FEM is a numerical method that is used to solve Laplace and Poisson type differential equations. Torque and flux density distribution of a motor—loaded or not—can be calculated according to the material properties and physical dimensions of the motor. The relationship that is extracted from Maxwell's electromagnetic equations and which can be solved by FEM is given in Eq. (7).

$$-\frac{1}{\mu_0}\nabla^2 A = J + \nabla \times M \tag{7}$$

Here $A$, $J$, and $M$ are the vector potential, excitation current density, and magnetization, respectively.

The vector potential values at any points on the motor can be obtained from the solution of Eq. (8) with FEM.

$$[S_{ij}]\,[A_j] = [r_i] \tag{8}$$

$[A_j]$ is the node potentials vector, where $[S_{ij}]$ is the finite element stiffness matrix. The mesh in the region of solution changes depending on the materials used in the motor and relative positions of the rotor and stator. Moreover, the stiffness matrix given in Eq. (8) becomes nonlinear since the magnetic permeabilities of the

materials used in the rotor and stator are nonlinear. $[r_i]$ is related to the mesh in the region of solution and magnetic properties of the materials used in the motor. It is a function of the excitation current.

It is necessary to know well the geometry of the motor and the properties of the materials used in the motor in order to analyze a motor with FEM. The PMSM produced by us is a motor having 12 slots and 4 poles and the properties of the plates and magnets, winding forms, and number of turns are known. The front view of the PMSM to be investigated with FEM and synchronous reference plane is shown in Figure 1a. The technical drawing of the motor, the B-H curve, and parameters are given in the Appendix.

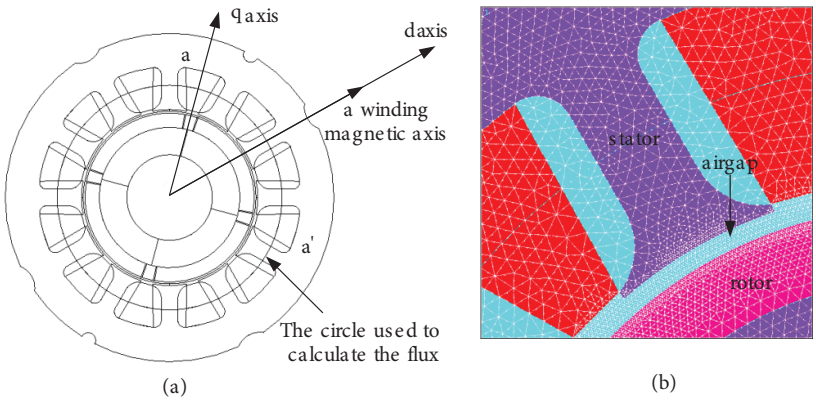


**Figure 1.** a) The schematic structure of the motor investigated by using FEM, b) The meshed model of the motor.

In this work the program ANSYS 10.0 is used to calculate the flux linkages produced by the windings. The calculation uses the vector potential values on the nodes in a circle that passes through the middle of the stator slots.

This circle is used in both the calculations of the average values of the magnetic vector potential values of each of the motor windings and the winding area, which is necessary to calculate the winding fluxes. A line that consists of the nodes on this circle is defined for each phase winding and this line is not changed during the FEM calculations for every position of the rotor. While rotating the rotor with increments of one degree, the stator and rotor meshes remain constant. Only the mesh in the air gap is changed. The same mesh is used with the help of a line consisting of the nodes in another circle passing through the middle of the air gap, just like the circle in the stator. Therefore, while the coordinates of the nodes in the rotor region rotate by one degree, the coordinates of the nodes building the line defined in the air gap remain constant.

After defining the geometry of the motor and the magnetic properties of the materials used, the mesh is produced as shown in Figure 1b. Triangular elements, which are widely used, are preferred to construct the mesh. The B-H curve of the steel plates used in the stator and rotor is used in the calculation of the stiffness matrix.

In this work, no windings of the motor are excited and winding flux linkages come from only the permanent magnets on the rotor during the FEM calculations. The winding flux linkages of the motor are calculated from Eq. (9) by using the vector potential values of the nodes on the predefined line using FEM for every incremental angle of one degree.

$$\lambda = \left[ \frac{\iint_{s_1} A_1 ds}{s_1} - \frac{\iint_{s_2} A_2 ds}{s_2} \right] l \tag{9}$$

Here $l$ represents the length of the motor and $s_1$ and $s_2$ represent the total areas carrying positive and negative currents, respectively.

In practice, a skew with a certain angle is given to the stator slots to make the air gap flux sinusoidal. This skew normally is not considered in 2D FEM analysis and this needs 3D analysis. However, in this work the skew is also taken into account with the proposed approach by using Eq. (10) in the calculation of the fluxes.

$$\lambda_{m_{abc}}(\theta(k)) = \frac{1}{\theta_{skew}} \sum_{\theta=\theta(k)}^{\theta_{(k)}+\theta skew} \lambda_{m_{abc}}(\theta)(k = mod(0,1,2,360)) \tag{10}$$

The value of the flux at any $\theta(k)$ angle taking the skew into account is calculated by the average of the fluxes from that angle to the angle of $\theta_{(k)} + \theta_{skew}$. By this way, there is no need for complicated and time consuming 3D analysis to take the effect of the skew into account.

The flux linkage of a phase winding calculated with FEM when the rotor is rotated by increments of one degree is shown in Figure 2a. It is seen in Figure 2a that the winding flux linkage created by the motor magnets do not vary as an exact sinusoidal. In Figure 2b it is seen that the flux linkages obtained from FEM calculations can be modelled by Fourier expansion approach. The modelling of the flux linkages with the Fourier expansion approach is given in Eq. (11).

$$\lambda_{mp} = \sum_{n=1}^{\infty} \lambda_{m(2n-1)} \cos((2n-1)\theta_r) \tag{11}$$

Here n represents the harmonic degree and p represents number of the stator phases. The harmonic components in Eq. (11) for n = 3 and multiples of 3 are zero for balanced - loaded motors.

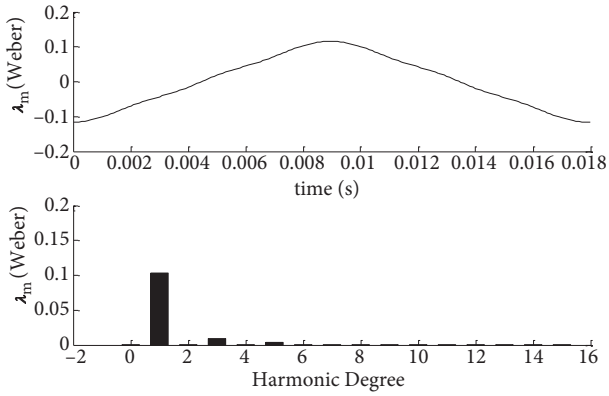


**Figure 2.** a) The flux linkage of a winding, b) The Fourier analysis of the flux linkage.

The stator reference plane transform of the flux model in Eq. (11) is given in Eqs. (12) and (13) up to the 13th harmonic.

$$\lambda_{m\alpha} = \lambda_{m1}\cos(\theta_r) + \lambda_{m5}\cos(5\theta_r) + \lambda_{m7}\cos(7\theta_r) + \lambda_{m11}\cos(11\theta_r) + \lambda_{m13}\cos(13\theta_r) \tag{12}$$

$$\lambda_{m\beta} = -\lambda_{m1}\sin(\theta_r) + \lambda_{m5}\sin(5\theta_r) - \lambda_{m7}\sin(7\theta_r) + \lambda_{m11}\sin(11\theta_r) - \lambda_{m13}\sin(13\theta_r) \tag{13}$$

The stator reference plane flux and torque equations of the PMSM under investigation are given in Eqs. (14)–(16).

$$\lambda_{md} = \lambda_{m1} + \lambda_{m5}\cos(6\theta_r) + \lambda_{m7}\cos(6\theta_r) + \lambda_{m11}\cos(12\theta_r) + \lambda_{m13}\cos(12\theta_r) \tag{14}$$

$$\lambda_{mq} = -\lambda_{m5}\sin(6\theta_r) + \lambda_{m7}\sin(6\theta_r) - \lambda_{m11}\sin(12\theta_r) + \lambda_{m13}\sin(12\theta_r) \tag{15}$$

$$\begin{aligned} T_e &= \tfrac{3P}{2}\left[i_q\left(\lambda_{m1} + \lambda_{m5}\cos(6\theta_r) + \lambda_{m7}\cos(6\theta_r) + \lambda_{m11}\cos(12\theta_r) + \lambda_{m13}\cos(12\theta_r)\right)\right. \\ &\quad \left. -i_d\left(-\lambda_{m5}\sin(6\theta_r) + \lambda_{m7}\sin(6\theta_r) - \lambda_{m11}\sin(12\theta_r) + \lambda_{m13}\sin(12\theta_r)\right)\right] \end{aligned} \tag{16}$$

The mathematical expressions of the stator winding flux linkages obtained from FEM can be used in the motor model and this model provides benefits in preventing torque ripples and sensorless control. However, the harmonic degree of the model must be limited in control procedures using digital signal processors. This causes some truncation errors in digital control. In order to prevent these truncation errors, the stator flux linkages may be modelled with an ANN as proposed in this work.

## 4. Obtaining the rotor position with an ANN from the winding flux linkages

ANNs are the systems that are used to model how a brain performs a function. An ANN having a sufficient number of neurons learns the information with a small error and generalizes it after its training. Numbers of input and output neurons of ANN are the same as the modelled system has. The number of hidden layer neurons depends on the problem and is determined by trial and error method. However, a larger number of hidden layer neurons increases the accuracy of the model, while decreasing the speed of the control system. Training is the adjustment of the connection weights of the neurons of the ANN according to the samples of sufficient number taken from the problem under concern. ANNs are used for the systems that cannot be expressed by mathematical equations or that can be expressed by complex equations that cannot be solved by a processor. Furthermore, ANNs are more widely used in motor control methods since they are less influenced by the variations of parameters and are easier to perform as compared to the other methods in real-time applications.

The structure of the ANN used in this work to predict the rotor position of the PMSM is given in Figure 3. It is a feed forward ANN having 3 neurons for the phase fluxes in the input layer, 9 neurons in the hidden layer, and 1 neuron for rotor position in the output layer. The flux values obtained from the motor are used as the training information for ANN. The ANN used to control the motor is trained off-line by using a back propagation algorithm. After the ANN has been trained with different values of error tolerance, it is examined with the experimental test data to ensure that it performs well enough. The value of error tolerance in the possible shortest time has been determined as $10^{-8}$. The ANN Tansig, tansig, and purelin functions are used sequentially as the activation functions.

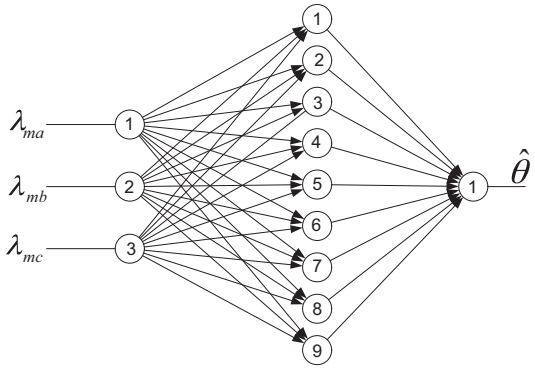


**Figure 3.** The structure of FEM based ANN.

The PMSM is rotated with an angular speed of 109 rad/s by means of a DC motor connected to its rotor shaft and the induced voltages on its windings are measured in order to show the performance of the ANN. The variations in the measured voltages with respect to each other are shown in Figure 4 as transformed to the stator reference plane. It is seen from Figure 4 that the flux waveform of the PMSM used in this work is not an exact sinusoidal.

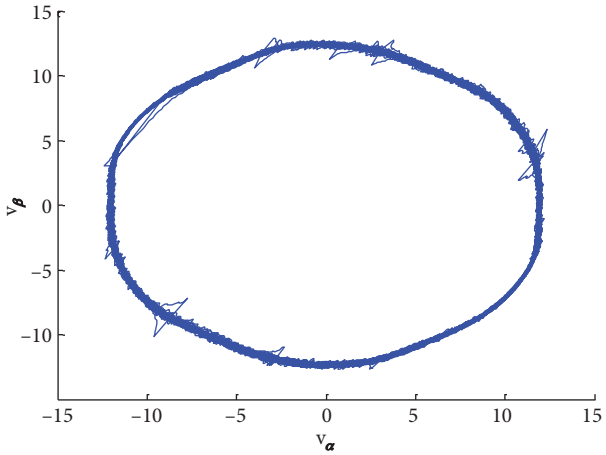


**Figure 4.** The variations in $v_\alpha$ and $v_\beta$.

The flux linkages given in Figure 5a are obtained by integrating these voltages measured experimentally. These flux linkages are applied to the ANN. The rotor positions estimated by the ANN as compared with experimentally measured position of the rotor are given in Figure 5b. It is seen from Figure 5b that the output of the ANN (dashed line) follows the measured rotor position. This means that the theoretical and experimental flux models agree with each other.

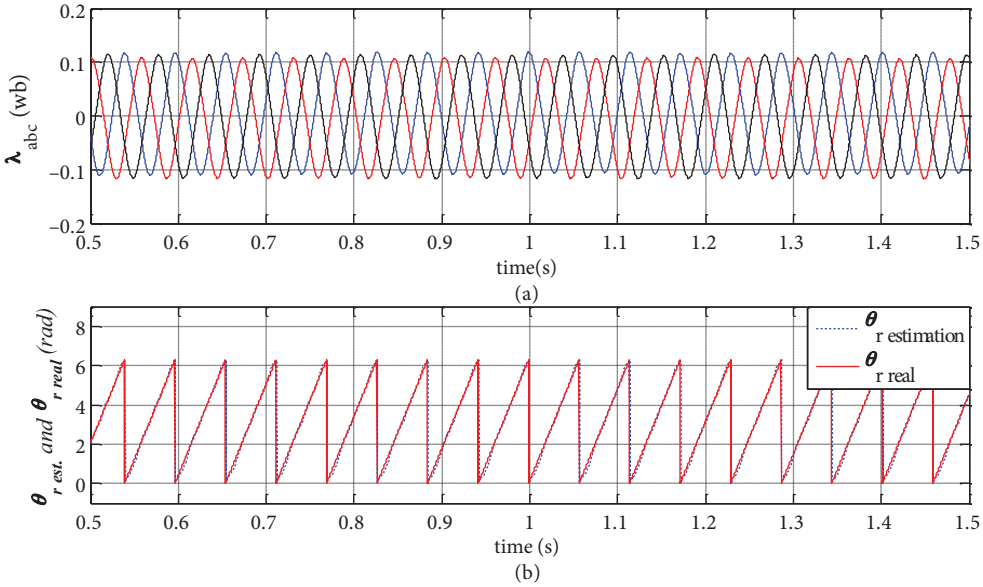


**Figure 5.** a) Measured fluxes, b) The estimated and measured rotor positions.

The ANN in the observer is trained using MATLAB/Neural Network Toolbox by means of the data obtained from FEM.

The real-time application of the ANN using the weights and biases obtained with this training is performed by C programming using the S-function of the Slave DSP TMS320F240 digital signal processor. By this way, it becomes possible to operate in a very short sampling time.

## 5. Flux linkage observer for a PMSM with sinusoidal flux-distribution

The block diagram of flux linkage observer for a PMSM with sinusoidal flux-distribution is given in Figure 6. In this method, which is well known as the traditional flux linkage method, the fluxes produced by permanent magnets are assumed to be exact sinusoidal in this method and the rotor position can be obtained by inverse tangent function [21]. The traditional flux linkage method based on the phasor diagram of a PMSM is shown in Figure 6.

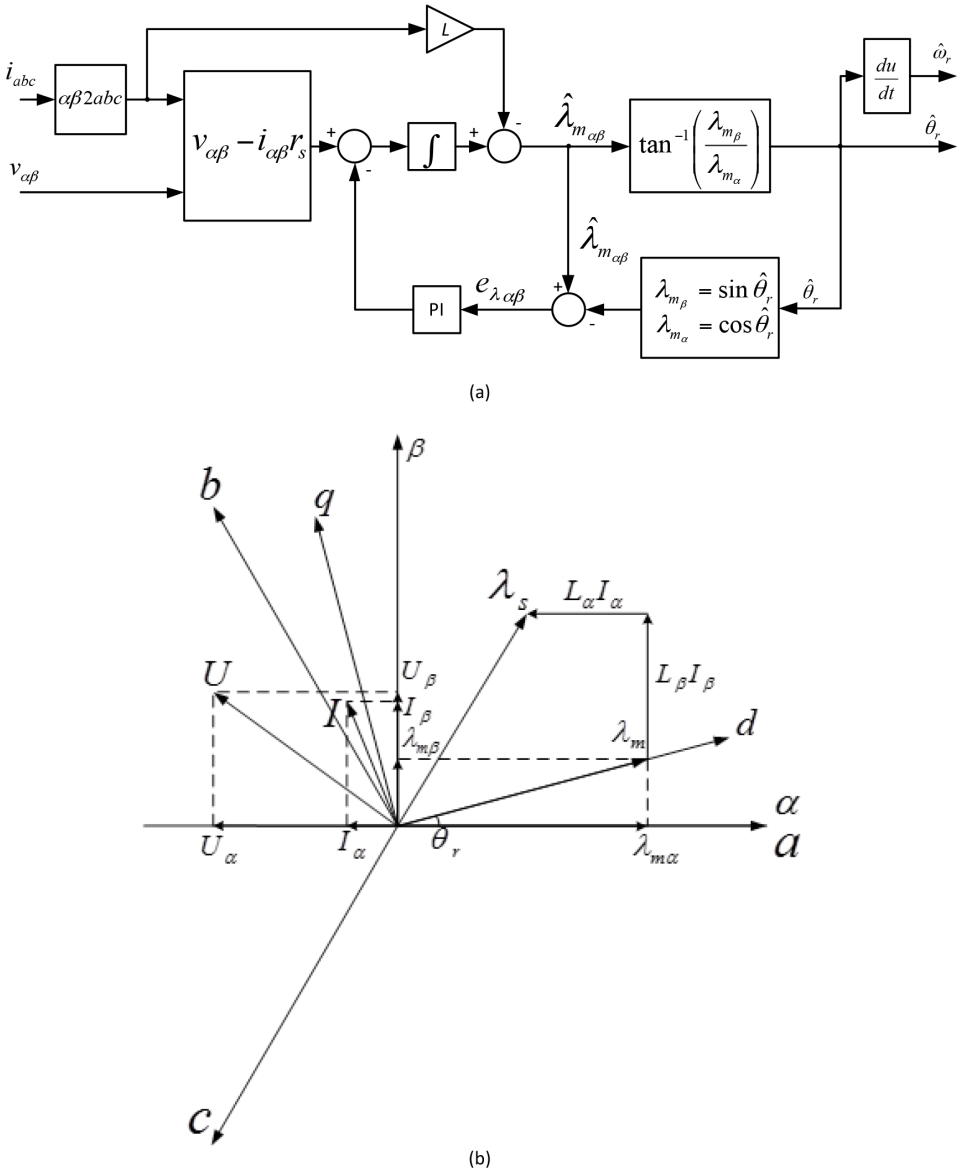


**Figure 6.** a) The block diagram of flux linkage observer for PMSM with sinusoidal flux-distribution,b) Phasor diagram of PMSM.

The alpha–beta components of the measured current and applied voltage are obtained by using Clarke transform equations. The alpha–beta components of stator flux linkage are obtained from Eqs. (17) and (18).

$$\lambda_\alpha = \lambda_{\alpha 0} + \int_0^t (v_\alpha - i_\alpha r_s)\, dt \tag{17}$$

$$\lambda_\beta = \lambda_{\beta 0} + \int_0^t (v_\beta - i_\beta r_s)\, dt \tag{18}$$

Here $\lambda_{\alpha 0}$ and $\lambda_{\beta 0}$ are the initial values of alpha–beta flux component. A method has been used to overcome the shifting problem of the integrator. Then the alpha–beta components of the magnet flux are calculated from Eqs. (19) and (20).

$$\lambda_{m\alpha} = \lambda_\alpha - i_\alpha L_\alpha \tag{19}$$

$$\lambda_{m\beta} = \lambda_\beta - i_\beta L_\beta \tag{20}$$

These flux components are assumed to be exactly sinusoidal in the traditional flux linkage method. Therefore, the rotor position is directly extracted from Eq. (21).

$$\theta_r = arctan\left(\frac{\lambda_{m\beta}}{\lambda_{m\alpha}}\right) \tag{21}$$

Estimated speed is calculated from Eq. (22).

$$\omega_r = \frac{d\theta_r}{dt} \tag{22}$$

## 6. FEM based ANN observer

The block diagram of the proposed FEM based observer is shown in Figure 7. Measured PMSM currents and stator reference plane voltages, which are the input of the space vector PWM generator, are given to the observer as input. These voltages are calculated. Voltage sensors are not used since an economical driver is desired. Calculated $v_{\alpha\beta}$ voltage values are used in the calculations by transforming them into the *abc* reference plane. The derivatives of the stator flux linkages are calculated as seen in Eq. (23) [22].

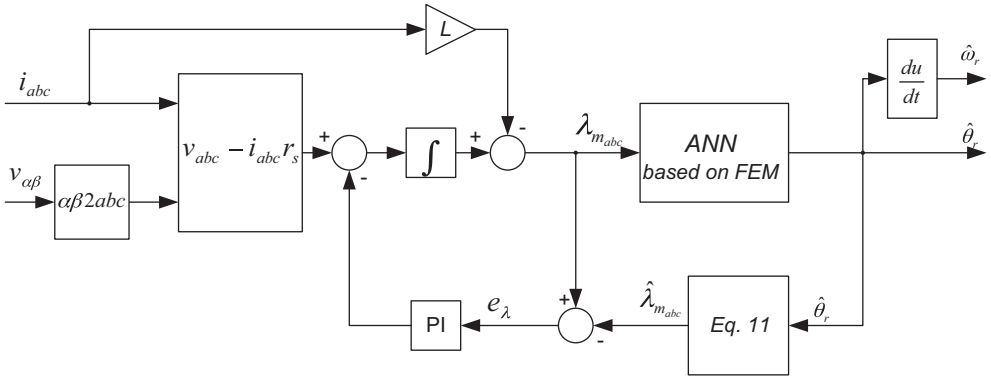


**Figure 7.** The structure of the FEM based ANN observer.

$$\frac{d\lambda_{abc}(\theta_r)}{dt} = v_{abc} - i_{abc}r_s \tag{23}$$

$$\lambda_{abc} = i_{abc}L_{abc} + \lambda_{m_{abc}}(\theta_r) \tag{24}$$

To obtain winding flux linkages, the integral must be evaluated and in any integration the most important problem is the shift arising from the initial value of the problem. A PI controller shown in Figure 7 is utilized to overcome this problem. This controller is not only used to prevent the shift, but it is also used to correct the estimated rotor position from the FEM based ANN observer. Therefore, errors occurring because of the variations in the motor parameters are corrected. For this reason, the components up to the 13th harmonic of Eq. (11) are used. This is necessary to get information about how the waveform of the calculated fluxes must be with respect to the rotor position estimated by the ANN. The use of the harmonics up to 13th degree does not cause any significant errors, since that information is not used to estimate rotor position directly by the ANN.

The error $e_\lambda$ between measured $\lambda_{m_{abc}}$ and calculated $\hat{\lambda}_{m_{abc}}$ with Eq. (11) according to the estimated rotor position is given as input to the PI controller to be used as the correction term in flux calculations. The variations in motor parameters also result in errors in the flux calculations causing wrong position information. The information of position is obtained from Eq. (11) and flux corrections are made. Thus the accuracy of the proposed method does not depend on the variations in motor parameters. The output of the observer is the rotor position estimation and the angular speed is its derivative with respect to the time.

## 7. Proposed sensorless control method

A block diagram of the field oriented control of a PMSM without speed and position sensors is shown in Figure 8. The d axis is made coinciding with the permanent magnet flux phasor; therefore the q axis is coinciding with the back emf phasor. Rotor position information is needed to transform phase currents into $i_d$ and $i_q$ currents in the rotor reference plane to perform current control. This information is obtained from a FEM based ANN observer instead of position and speed sensors. To control the currents $i_d$ and $i_q$ independently and to get a good performance, decoupling terms that are the derivatives of Eqs. (12) and (13) are added to the output of the current controller.

Inverter control signals are created by space vector PWM (SVPWM) by using $V_\alpha$ and $V_\beta$ voltages. The SVPWM is a PWM method implemented by digital processors. The SVPWM has a better harmonic distortion than the sinusoidal PWM. Moreover, the maximum voltage value obtained from the inverter in the SVPWM is higher than that of the sinusoidal PWM. However, there is a disadvantage in that the calculation time of the SVPWM for signal generation is greater since it includes complex equations.

Probable discrete space vectors in the three phase inverter and reference voltage vector are shown in Figures 9a and 9b, respectively.

The general expression of discrete space vectors is given in Eq. (25). Here $v_{dc}$ is dc bus voltage of the inverter and $k$ is the sector in which the reference voltage vector exists.

$$v_k = \frac{2}{3}v_{dc}e^{j(k-1)\frac{\pi}{3}} \tag{25}$$

The reference voltage vector in the SVPWM inverter is the average of neighboring two active vectors and two zero vectors in the switching period $T_s$. If $T_s$ is sufficiently small, $v_{ref}$ given in Eq. (26) does not change during the switching period.

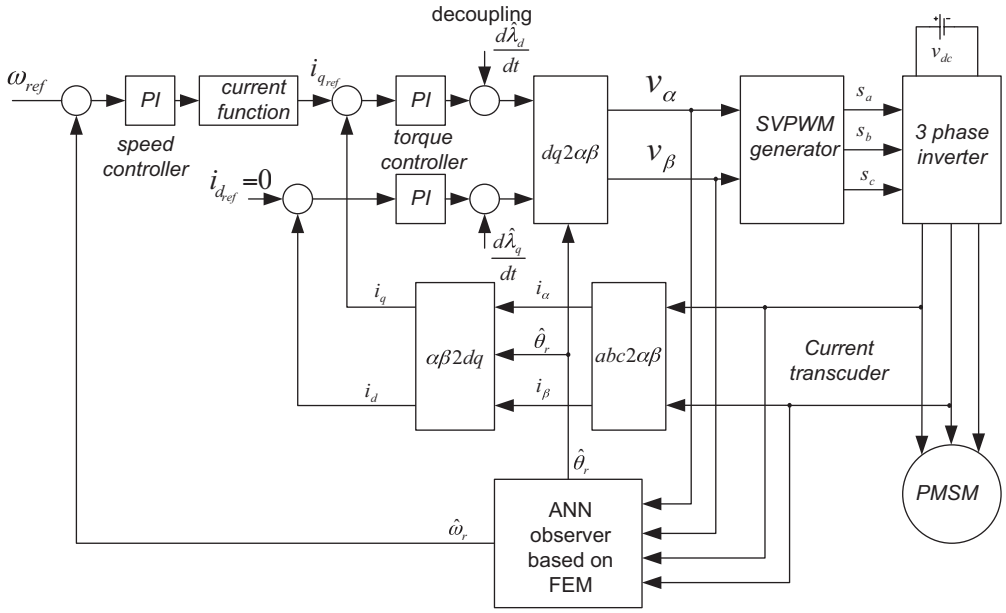


**Figure 8.** The block diagram of speed and position sensorless field oriented control of PMSM.

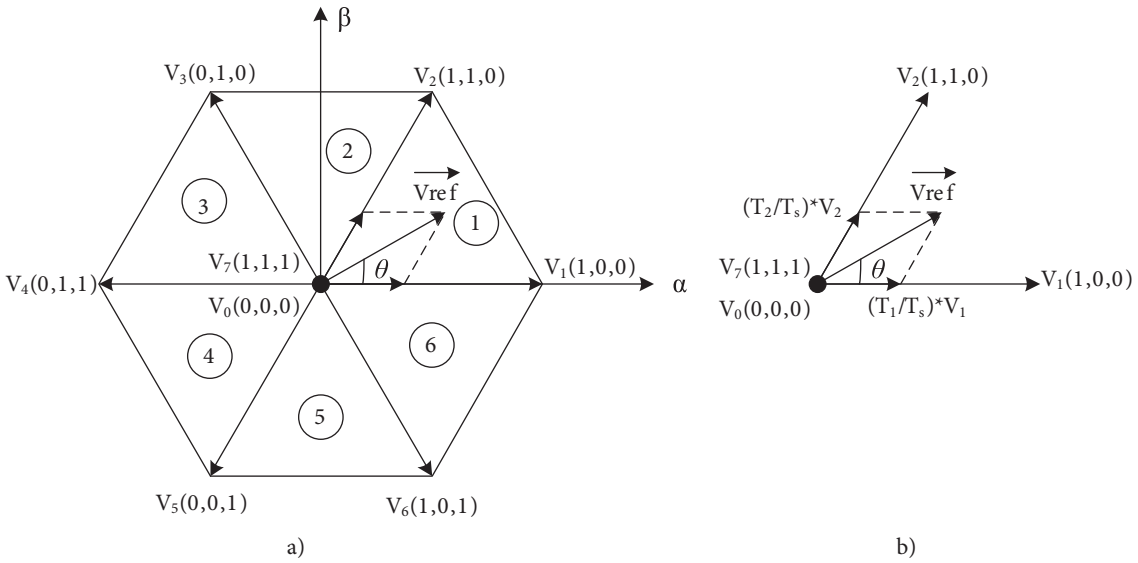


**Figure 9.** a) Space vectors, b) Reference voltage vector.

$$v_{ref} = v_k \frac{T_k}{T_s/2} + v_{k+1} \frac{T_{k+1}}{T_s/2} \tag{26}$$

Three phase PWM signals are shown in Figure 10 while the reference space voltage vector is in the first sector.

The time values $T_k$ and $T_{k+1}$ needed to obtain PWM signal are calculated from Eq. (27).

$$\begin{bmatrix} T_k \\ T_{k+1} \end{bmatrix} = \frac{\sqrt{3}}{2} \frac{T_s}{V_{dc}} \begin{bmatrix} \sin \frac{k\pi}{3} & -\cos \frac{k\pi}{3} \\ -sin \frac{(k-1)\pi}{3} & \cos \frac{(k-1)\pi}{3} \end{bmatrix} \begin{bmatrix} v_\alpha \\ v_\beta \end{bmatrix} \tag{27}$$

Here $v_\alpha$ and $v_\beta$ represent stator reference plane voltages.

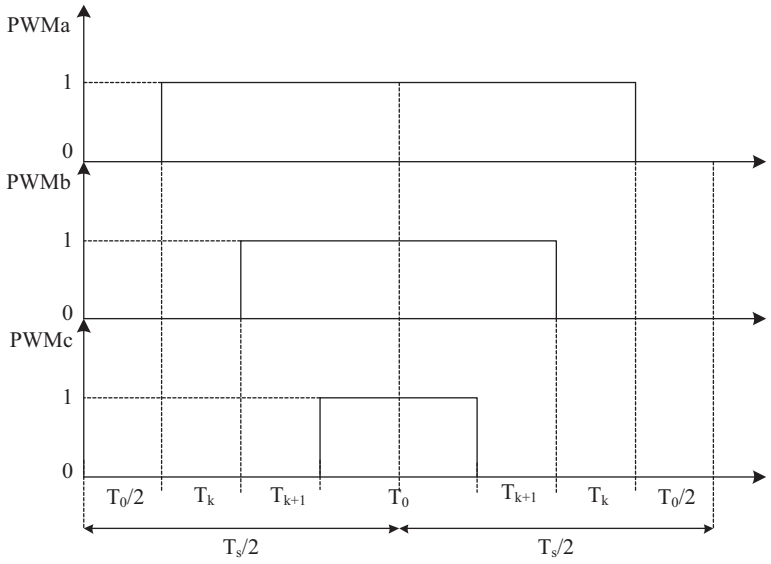


**Figure 10.** PWM signals while the reference space vector is in the first sector.

The proposed FEM based ANN observer in this paper may be applied to any permanent magnet motor having arbitrary flux wave shape.

## 8. Implementation of sensorless vector control of a PMSM

### 8.1. Experimental setup

The experimental setup consists of a 650 W PMSM, IGBT based PWM voltage-source inverter, incremental encoder (used only for comparison purposes), two current sensors, dSPACE ACE-Kit 1103 with DS1103 R&D Controller Board, and a PC. The DS1103 PPC Controller Board is designed especially for development of high-speed multivariable digital controllers and real-time simulations in various fields. It is a complete real-time control system based on a PowerPC processor. The board includes a slave-DSP subsystem based on the Texas Instruments TMS320F240 DSP microcontroller. In this work, operation at a higher switching frequency is achieved with generation of ANN and PWM by means of C programming of this slave DSP directly. The board is equipped with 32 MB boot flash, 96 MB global DRAM, twenty 16-bit analog-to-digital converters, eight digital-to-analog channels (16-bit), three-phase PWM outputs plus four single PWM outputs, twenty bits of digital I/O, incremental encoder interface, serial interface, and CAN bus interface. The board is inserted in a dSPACE expansion box communicating with the host PC via an ISA-bus extension (DS817). A fiber-optic wire is used for communication between DS817 and dSPACE expansion box. The PC is used for software development and visualization of results. The experimental setup of the field oriented position and speed sensorless control of the PMSM is shown in Figure 11.

The field oriented position and speed sensorless control algorithm of the PMSM is formed in MATLAB/Simulink software and uploaded to DS1103. Measurement of motor currents is performed using LEM current sensors with two analogue inputs with sampling frequency 5 kHz.

The speed is measured using an incremental encoder interfaced to a DSPACE quadrature decoder with sampling frequency 5 kHz. The control of switching elements of the inverter is performed by SVPWM with 5 kHz switching frequency. Control of experiments, visualization, and data acquisition are realized by dSPACE software Control Desk Developer.

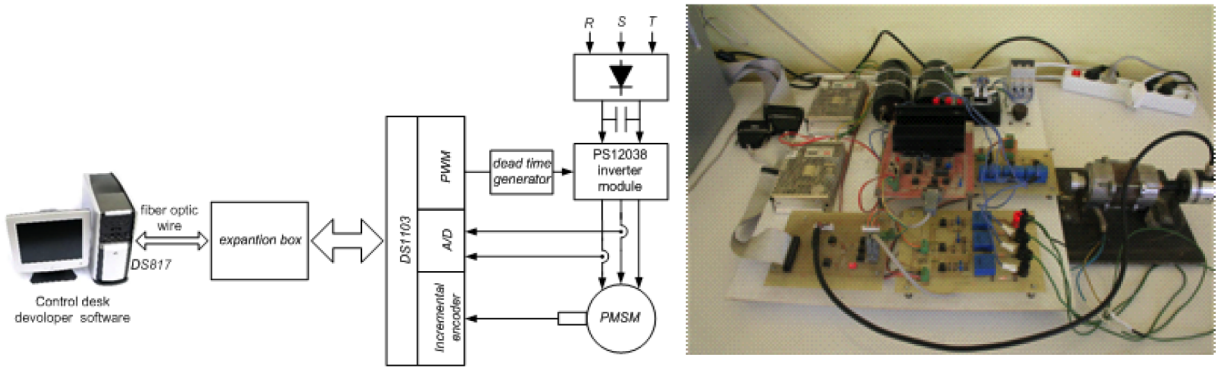


**Figure 11.** The experimental setup for the field-oriented control of the PMSM.

The PWM voltage source inverters have nonlinearities known as DC link voltage ripple, dead time, and switching elements (diodes and IGBTs) voltage drop. The inverter nonlinearity compensation methods discussed in detail in [23] are applied to the driver system to obtain better performance.

### 8.2. Experimental results

The experimental results are achieved in the experimental setup described above to prove the validity of the sensorless vector control of a PMSM with nonsinusoidal flux using an observer based on FEM. An incremental encoder with 2048 pulses is used to measure the rotor position and speed and compare with the estimated values. However, this information from the measurements is not used in the vector control of the PMSM.

The measured flux values, estimated rotor position from the ANN, and measured rotor position values are given in Figures 12a and 12b, respectively. The PMSM initially has been run at 50 rad/s while it has been controlled sensorless; it is then accelerated up to 100 rad/s at 1.2 s. The ANN has estimated the rotor position correctly at both speeds and this estimation of rotor position has been used in closed loop sensorless control.

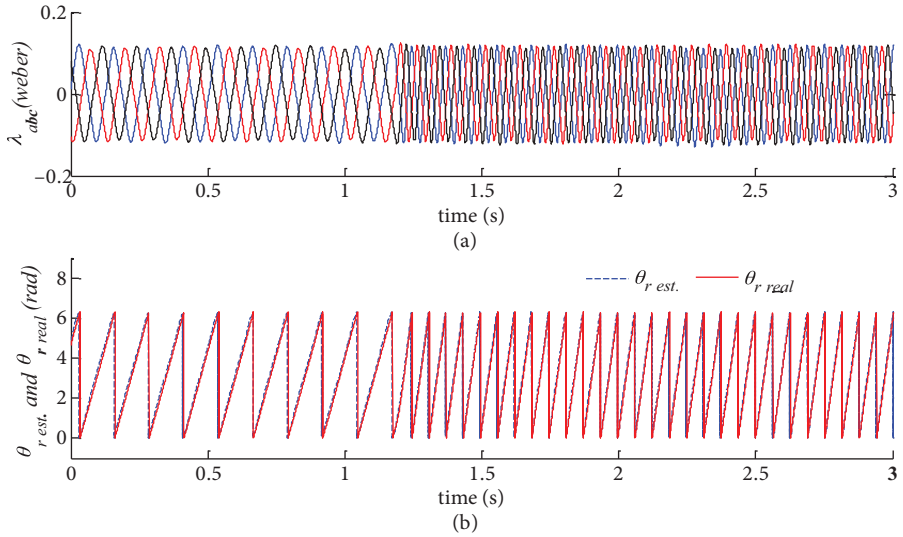


**Figure 12.** a) Inputs of ANN, b) Real rotor position and rotor position estimated by the ANN.

Experimental results of the field oriented control of a PMSM using rotor position and speed estimation from a FEM based observer in unloaded conditions at low and high speeds are given in Figure 13. Measured

rotor speed, estimated speed by the FEM based observer, and error between measured and estimated speeds are given in Figures 13a and 13b, respectively.

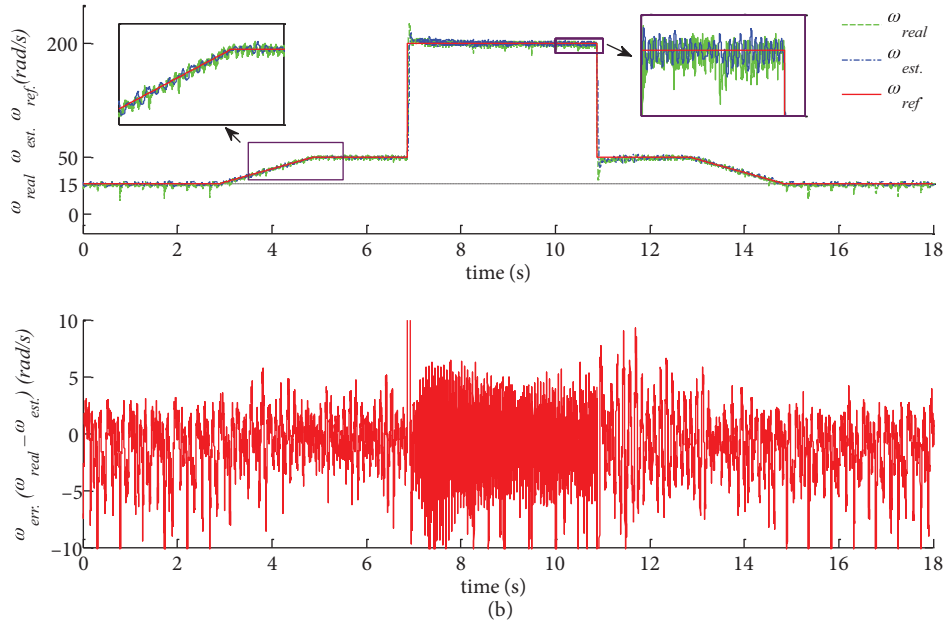


**Figure 13.** Performance of the FEM based observer at different speeds.

The proposed observer can predict the rotor position and speed correctly even at low speeds such as 15 rad/s as can be seen from Figure 14.

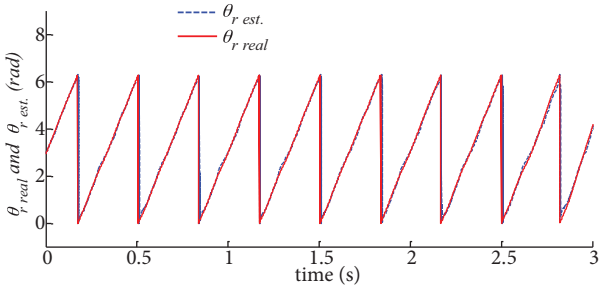


**Figure 14.** Measured and estimated rotor positions at low speed (15 rad/s).

The PMSM is loaded with 0.5 Nm torque after about 8.2 s later when it is running sensorless at 50 rad/s constant angular speed and the results are obtained using a control desk. Measured rotor speed by the speed sensor, estimated speed by the FEM based ANN observer, and the difference between measured and estimated speeds are given in Figures 15a and 15b, respectively.

Figure 16 shows the measured and estimated rotor positions in the time interval that the PMSM is loaded.

Figure 17 shows the PMSM's measured $i_d$ and $i_q$ currents in the rotor reference plane in under-load experiment.

Finally, the traditional flux linkage method and the proposed method are compared by using the experimental results to prove the validity of the FEM based observer. For this, the sensorless field oriented controls of a PMSM are performed with both methods. The motor is loaded with a torque of 0.5 Nm during a time

period of 0.8 s while it is running sensorless at a reference speed of 200 rad/s in both experiments. Reference, measured, and estimated speeds by using the traditional flux linkage method are shown in Figure 18a and the difference between the actual and estimated speeds is shown in Figure 18b. The reference, measured, and estimated speeds obtained by using the proposed method are shown in Figure 18c and the error for this method is shown in Figure 18d. As Figure 18b and Figure 18d are compared with each other, it can be seen that the proposed method has a better speed estimation than the traditional flux linkage method.

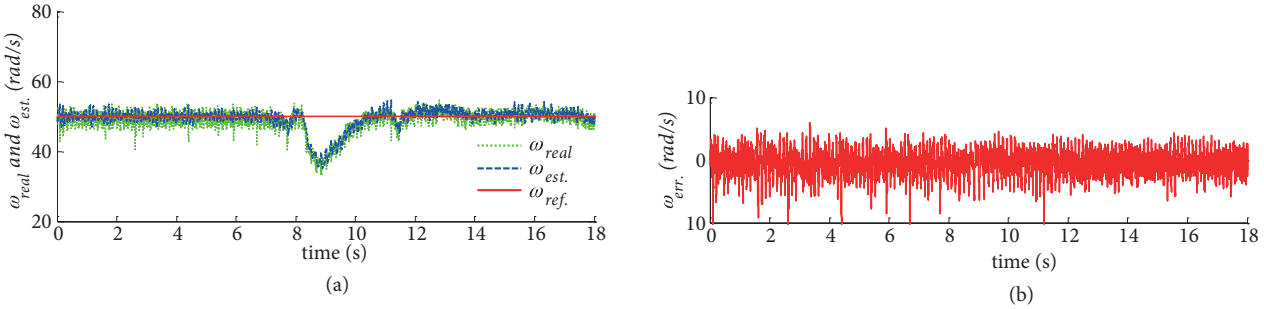


**Figure 15.** Rotor speeds under the sensorless field oriented control of PMSM with load.

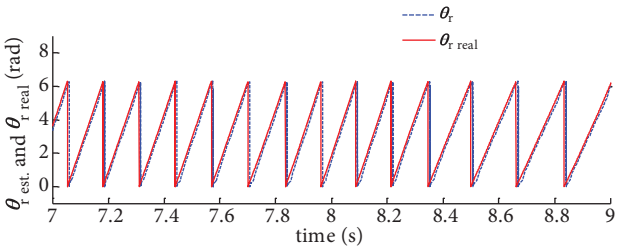


**Figure 16**. The measured and estimated rotor positions of the PMSM when it is loaded.

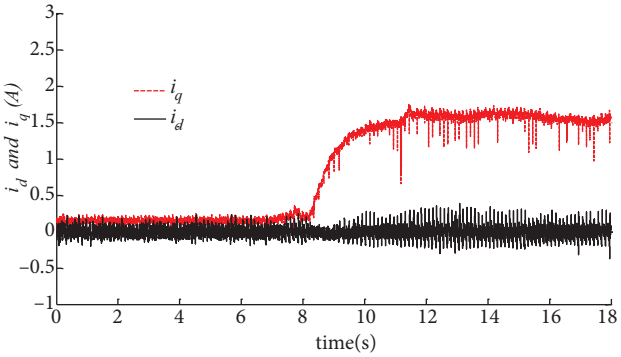


**Figure 17.** Rotor reference plane $i_d$ and $i_q$ currents of the motor for under-load experiment.

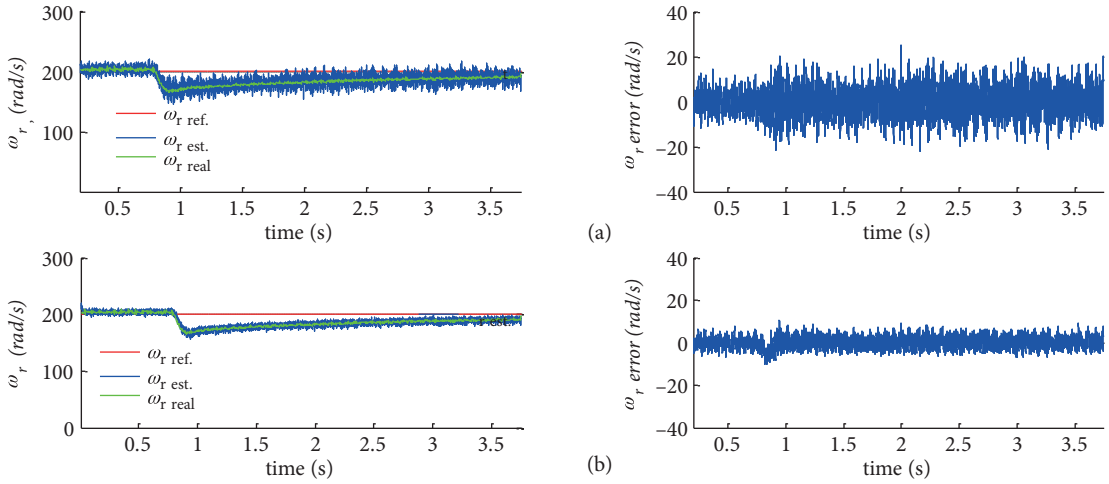


**Figure 18.** a) The plots of the rotor speed and speed error obtained from the flux linkage observer for PMSM with sinusoidal flux-distribution, b) The plots of the rotor speed and speed error obtained from the FEM based ANN observer.

The estimated rotor position by using the traditional flux linkage method and the measured rotor position are given in Figure 19a. The difference between the measured and estimated positions during 0.1 s is given in Figure 19b. In Figure 19c and 19d, the rotor positions obtained from the proposed sensorless control and position error are shown, respectively. It can obviously be seen that the position error of the FEM based ANN observer is smaller than that of the other method, and so the proposed method estimates the rotor position more accurately than the traditional flux linkage method.

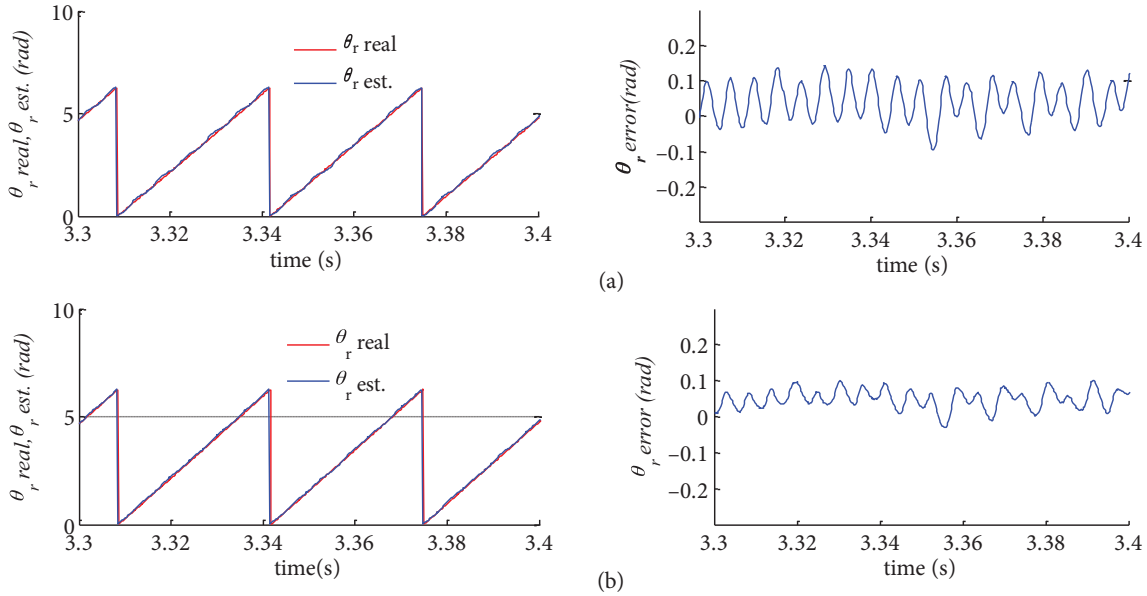


**Figure 19.** a) The rotor positions and position errors obtained from the flux linkage observer for PMSM with sinusoidal flux-distribution, b) The rotor positions and position errors from the FEM based ANN observer.

### 8.3. Discussion and conclusion

In our study, field oriented control of a PMSM having a nonsinusoidal flux-distribution has been performed using a FEM based ANN observer. At first, the waveforms of the flux linkages created by permanent magnets in the rotor have been determined by using FEM. The ANN inside the suggested observer has been trained off-line according to this obtained waveform and then used to predict the rotor position. A PI controller has been used to overcome the shifting problem of the integrator in determination of the winding fluxes. This method can be applied to any PMSM having arbitrary flux wave shape. While analyzing a PMSM with FEM, it may be a disadvantage of the method to need information on motor dimensions and magnetic properties of the materials used. However, since PMSMs need a driver circuit to run, manufacturers also a construct driver circuit together with the PMSM and they have information necessary for the FEM. Therefore, the driver circuit of the PMSM can also be manufactured together appropriately for its flux waveform.

## References

[1] Rusong W, Slemon G. A permanent magnet motor drive without a shaft sensor. IEEE Trans. on Ind. Appl. 1991; 27: 1005-1011.

[2] Gumus B, Ozdemir M. Sensorless vector control of a permanent magnet synchronous motor with fuzzy logic observer. Electrical Engineering 2006; 88: 395-402.

[3] Göksu Ö, Hava AM. Experimental investigation of shaft transducerless speed and position control of ac induction and interior permanent magnet motors. Turk J Elec Eng & Comp Sci 2010; 18: 865-882.

[4] Matsui N. Sensorless PM brushless DC motor drives. IEEE T Ind Elect 1996; 43: 300-308.

[5] Acarnley PP, Watson JF. Review of position-sensorless operation of brushless permanent-magnet machines. IEEE T Ind Elect 2006; 53: 352-362.

[6] Zhiqian C, Tomita M, Doki S, Okuma S. An extended electromotive force model for sensorless control of interior permanent-magnet synchronous motors. IEEE T Ind Elect 2003; 50: 288-295.

[7] Kim H, Son J, Lee J. A high-speed sliding-mode observer for the sensorless speed control of a pmsm. IEEE T Ind Elect 2011; 58: 4069-4077.

[8] Hejny RW, Lorenz RD. Evaluating the practical low-speed limits for back-emf tracking-based sensorless speed control using drive stiffness as a key metric. IEEE T Ind App 2011; 47: 1337-1343.

[9] Genduso F, Miceli R, Rando C, Galluzzo GR. Back emf sensorless-control algorithm for high-dynamic performance pmsm. IEEE T Ind Elect 2010; 57: 2092-2100.

[10] Krishnan R, Vijayraghavan P. Fast estimation and compensation of rotor flux linkage in permanent magnet synchronous machines. In: IEEE ISIE'99 1999; 12–16 July; Bled, Slovenia: IEEE. pp. 661-666.

[11] Xi X, Meng Z, Yongdong L, Min L. On-line estimation of permanent magnet flux linkage ripple for pmsm based on a kalman filter. In: IEEE IECON'062006; 7–10 November; Paris, France: IEEE. pp. 1171-1175.

[12] Elbuluk M, Tong L, Iqbal H. Neural-network-based model reference adaptive systems for high-performance motor drives and motion controls. IEEE T Ind App 2002; 38: 879-886.

[13] Niazi P, Toliyat H. On-line parameter estimation of permanent magnet assisted synchronous reluctance motor drives. In: IEEE IEMDC'05 2005; 15–18 May; San Antonio, TX, USA: IEEE. pp. 1031-1036.

[14] Chan TF, Wang W, Borsje P, Wong YK, Ho SL. Sensorless permanent-magnet synchronous motor drive using a reduced-order rotor flux observer. IET Elect Power App 2008; 2: 88-98.

[15] Angelo CD, Bossio G, Solsona J, Garcia GO, Valla MI. A rotor position and speed observer for permanent-magnet motors with nonsinusoidal emf waveform. IEEE T Ind Elec 2005; 52: 807-813.

[16] Oksuztepe E, Omac Z, Kurum H. Sensorless vector control of PMSM with non-sinusoidal flux using observer based on FEM. Springer Electrical Engineering, 2014; 96: 227-238.

[17] Bouillault F, Marchand C. Improvement of servomotors control laws with the help of finite element method. IEEE T Mag 1995; 31: 2020-2025.

[18] Jahns T, Soong W. Pulsating torque minimization techniques for permanent magnet ac motor drives - a review. IEEE T Ind Elect 1996; 43: 321-330.

[19] Xu JX, Panda SK, Pan YJ, Lee TH, Lam BH. A modular control scheme for pmsm speed control with pulsating torque minimization. IEEE T Ind Elect 2004; 51: 526-536.

[20] Öksüztepe E, Kürüm H. Torque ripple minimization of permanent magnet synchronous motor with use of flux model composed of finite element. Erciyes University Fen Bilimleri Enstitüsü Dergisi 2009; 25: 120-133.

[21] Yuan Q, Yang Z, Lin F, Sun H. Sensorless control of permanent magnet synchronous motor with stator flux estimation. Journal of Computers 2013; 8: 108-112.

[22] Petrovi V, Stankovic AM. Modeling of pm synchronous motors for control and estimation tasks. In: The 40th IEEE Conference, Decision and Control 2001; 4–7 December, Orlando, Florida, USA: IEEE. pp. 2229-2234.

[23] Blaabjerg F, Pedersen JK, Thogersen P. Improved modulation techniques for PWM-VSI drives. IEEE T Ind Elect 1997; 44: 87-95.

## Appendix

The properties of the motor are given as follows:

Electrical and mechanical parameters:

The phase resistance, $r_s$: 2.6 Ω

The self-inductance, L : 3.63 mH

The inertia, J : 0.00257955 kg m$^2$

The damping coefficient, B : 0.00003743 Nm s/rad

The magnet flux, $\lambda_m$: 0.114 wb

Number of poles, 2P : 4

Magnet type: NeFeB Br = 1.3Tesla,

Number of turns (Per phase): 90

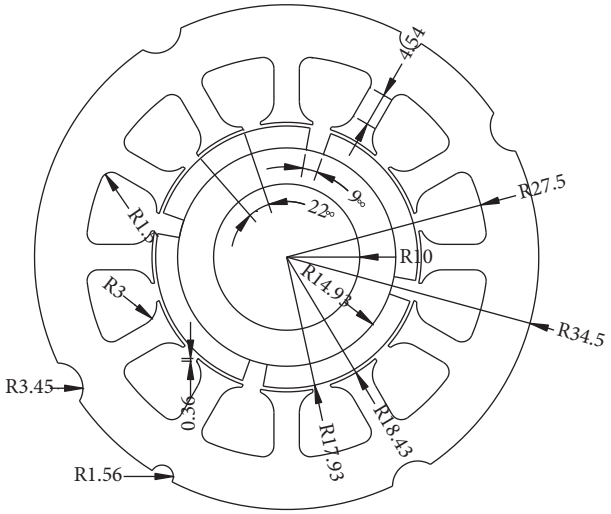


**Figure 1.** Technical drawing of the PMSM (dimensions are given in mm).

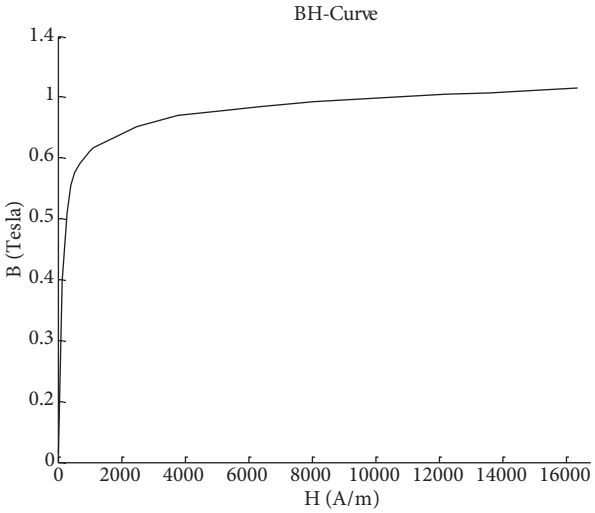


**Figure 2.** The B-H curve of the motor plates.